PHILOSOPHICAL TRANSACTIONS OF THE ROYAL SOCIETY A MATHEMATICAL, PHYSICAL & ENGINEERING SCIENCES

SLEEC: a space station ambulance

Terence R. F. Nonweiler

Phil. Trans. R. Soc. Lond. A 1999 **357**, 2157-2176
doi: 10.1098/rsta.1999.0426

THE ROYAL SOCIETY

SLEEC: a space station ambulance

By Terence R. F. Nonweiler

Victoria University, Wellington, New Zealand and
APECS Ltd, 3 Hawkley Hurst, Hawkley, Hants GU33 6NS, UK

The assembly of the International Space Station calls for many hundreds of hours of extra-vehicular activity, and for maintenance thereafter. Occupation will involve as many as eight residents at a time. This level of human activity introduces significant risk of injury or illness and the need to return the patient to Earth. This return must avoid delays in orbit and unnecessary physical stress to the patient.

SLEEC22 is a novel kind of 'space ambulance' based in orbit that is intended to return a patient and attendant back to Earth in a gentle winged descent, restricting the peak g experienced to less than a tenth above normal ground-level values. It allows a wider than usual 're-entry window' that would permit a landing at any of an extensive choice of airfields. It makes use of a lightweight waverider wing with only shallow anhedral and 'sharp' metallic leading edges. Cooling of the structure, both exterior and interior, is effected by conduction-assisted radiation.

Keywords: space station ambulance; waverider design; centreline stand-off angle; heat protection; choice of descent; low-g re-entry

1. Project definition

If an astronaut in a space station were to become so badly ill or injured as to need to be returned to Earth for treatment, how would this be achieved? In the present state of development, there would probably be considerable cost and delay in mounting a 'space rescue' mission from Earth. More likely, a ferry craft that had been used to bring crew to the station would be parked in orbit, and this would be used to return the ailing astronaut. In that event, presumably, an empty replacement ferry would then later need to be dispatched from Earth, for return of the remaining crew from the station; again a costly remedy.

This problem would be overcome much more easily if one or more specialized re-entry vehicles, relatively small and inexpensive, had already been carried up to the space station. There they would remain available for use as 'space ambulances', ready to return an ill or injured astronaut to Earth. In 1994 it was decided to study such a vehicle as part of a spaceplane review that was in hand for the British National Space Centre, and to treat the following design characteristics as definitive.

(1) The craft should have a span of less than 15 ft (4.5 m) and a length of less than 30 ft (9 m), so that it can be carried into orbit in one half of the Shuttle bay.

(2) It should re-enter carrying two people, one acting as an attendant to the other.

(3) The re-entry should deliberately avoid excessive g. This prescription later became quantified to a maximum of less than $1.1g$. Physiologically, there is no

'critical' limit, but the lower the safer. It would, in any event, depend upon the patient's medical problem, and an option to choose re-entry to trade off the 'g limit' against duration of descent would be desirable (though this has yet to be explored).

(4) The crossrange of the vehicle should be made as large as possible, with the intention of increasing the daily launch window of access to a particular airfield.

The accessibility of a particular airfield depends on its latitude as well as the inclination of the orbit from which re-entry is being made. However, as illustrated in figure 1, it is always increased by the crossrange capability during the glide. Not only is the frequency of occasions that a landing can be made on any particular airfield increased, but higher latitudes can be reached, allowing, perhaps, the choice of a larger number of alternative landing sites.

2. Choice of design for initial study

The limitation of acceleration and a high crossrange capability during the gliding re-entry both suggest the need for a craft with a high maximum lift-to-drag ratio, even though it may not be required throughout re-entry. It is the need for this high ratio that distinguishes the space ambulance from such craft as the Shuttle Orbiter (Walberg 1991), the HL-20 (Stone & Piland 1993), and the X-38 crew recovery vehicle demonstrator (Smith 1999). Due to its known advantages in developing a high lift-to-drag ratio, it was decided at the outset to consider a form of 'waverider' design, in which the bottom surface flow is contained behind a shock wave attached to the leading edge for much of the re-entry (Nonweiler 1959, 1990). For the purposes of this project study, the wing leading edges are treated as 'razor' sharp (or wedge-shaped), and, thus, strict flow containment is implied. However, it is realized that this is neither realistic nor necessarily desirable, and the design of the wing leading edge with a radius of perhaps up to several millimetres has already received detailed attention (Nonweiler *et al*. 1971), and is known to be advantageous for certain types of re-entry.

The thermal protection of such sharp edges is achievable by the provision of conducting material within the wing, which spreads out the region of high surface temperature over which radiative cooling is effective. This compares with, and differs from, the more usual method of thermal protection, by provision of a leading edge having significant radius of curvature: that is, a heavily rounded shape that spreads out the peak in aerodynamic heating. However, it is known that conduction-assisted cooling is only an adequate protection in re-entry if the heating rates are relatively low. This implies that the wing loading must be kept small, and a target figure of $70\ \mathrm{kg\ m^{-2}}$ ($14\ \mathrm{lb\ ft^{-2}}$) was chosen as compatible both with the limitation of size and the vehicle payload. Whether this target can be achieved will only be confirmed by an assessment of structure mass, which has yet to be done. However, it is believed that the loading is the same as that for the X-20 Dynasoar (Yoler 1961).

Figure 2 shows a three-view impression of the shape of the vehicle 'SLEEC22', selected for the first iteration of the project study, and current data relating to its geometry and mass are listed in Appendix A. (SLEEC is an acronym for slender lifting entry emergency craft.) We discuss below those particular features of the design that have received detailed attention. It must be emphasized that other features not mentioned are, meanwhile, necessarily tentative.

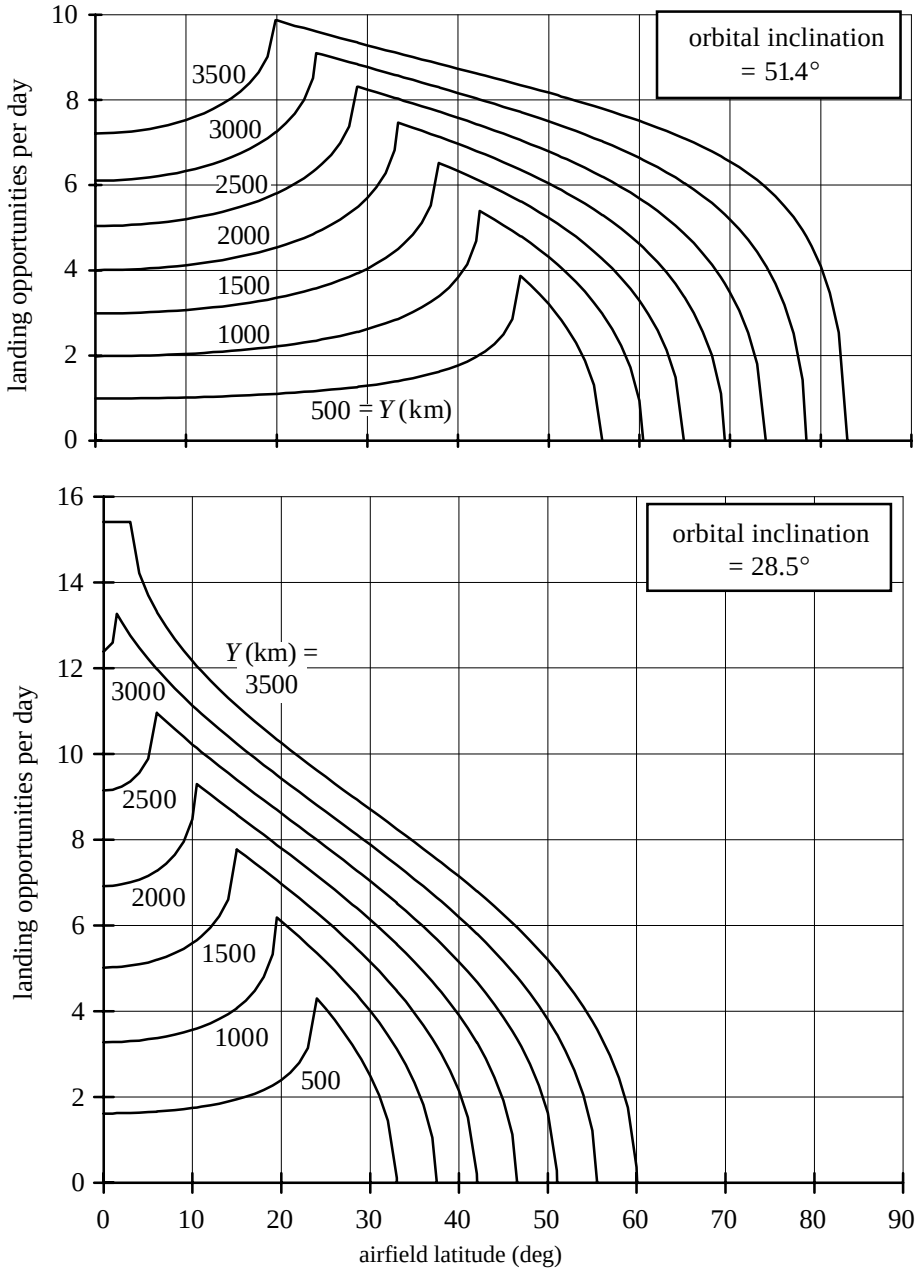

Figure 1. Effect of crossrange (Y), orbital inclination and airfield latitude on the average number of landing opportunities per day, when re-entering from an orbit of 450 km height.

3. Choice of centreline stand-off angle

For present purposes, we treat the wing as a delta whose underside has a slight inverted-V cross-section (as shown in figure 2). Its upper surface is supposed to be

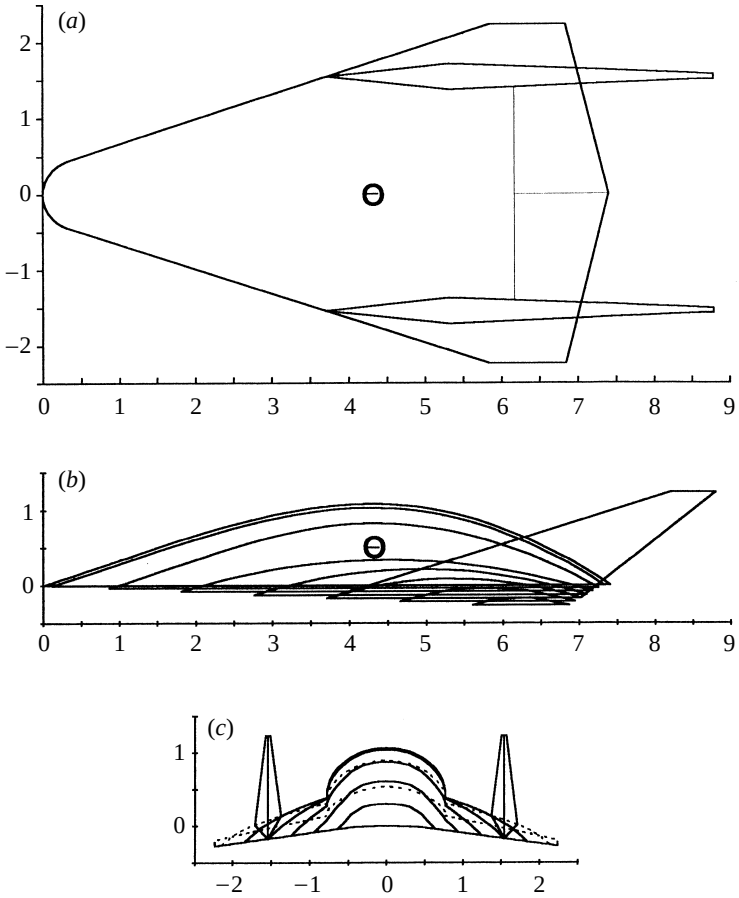

Figure 2. Shape of SLEEC22, selected for initial Project Study (for dimensions and masses, see Appendix A). (*a*) Plan view. (*b*) Longitudinal sections along and parallel to central plane of symmetry at 1 ft intervals spanwise (all measurements shown in metres). (*c*) Transverse sections across the span at 3 ft intervals (measurements in metres).

'in shadow' (i.e. nowhere forward facing). The wing incidence α (measured relative to the undersurface centreline) must, therefore, be no less than the leading-edge angle (measured in the streamwise direction). This latter was chosen as 17.4° to accommodate the cabin (as shown in figure 2).

The underside shock-wave configuration for such a wing depends upon the choice of the stand-off angle. This is the angle between the undersurface centreline and the plane of the leading edges. The shock configuration is detailed in the set of diagrams of figure 3. In each of these, the 'design condition', in which the shock wave lies in the plane of the leading edges, is shown by the full line. We have no interest in the flow conditions above this line where the undersurface shock will be attached but concave, lying above the plane of the leading edges. Rather, we require the aircraft to operate at Mach numbers below the design condition, where the shock remains attached but convex, extending below the plane of the leading edges. However, as figure 3 shows, with further decrease of Mach number, the shock will detach from the

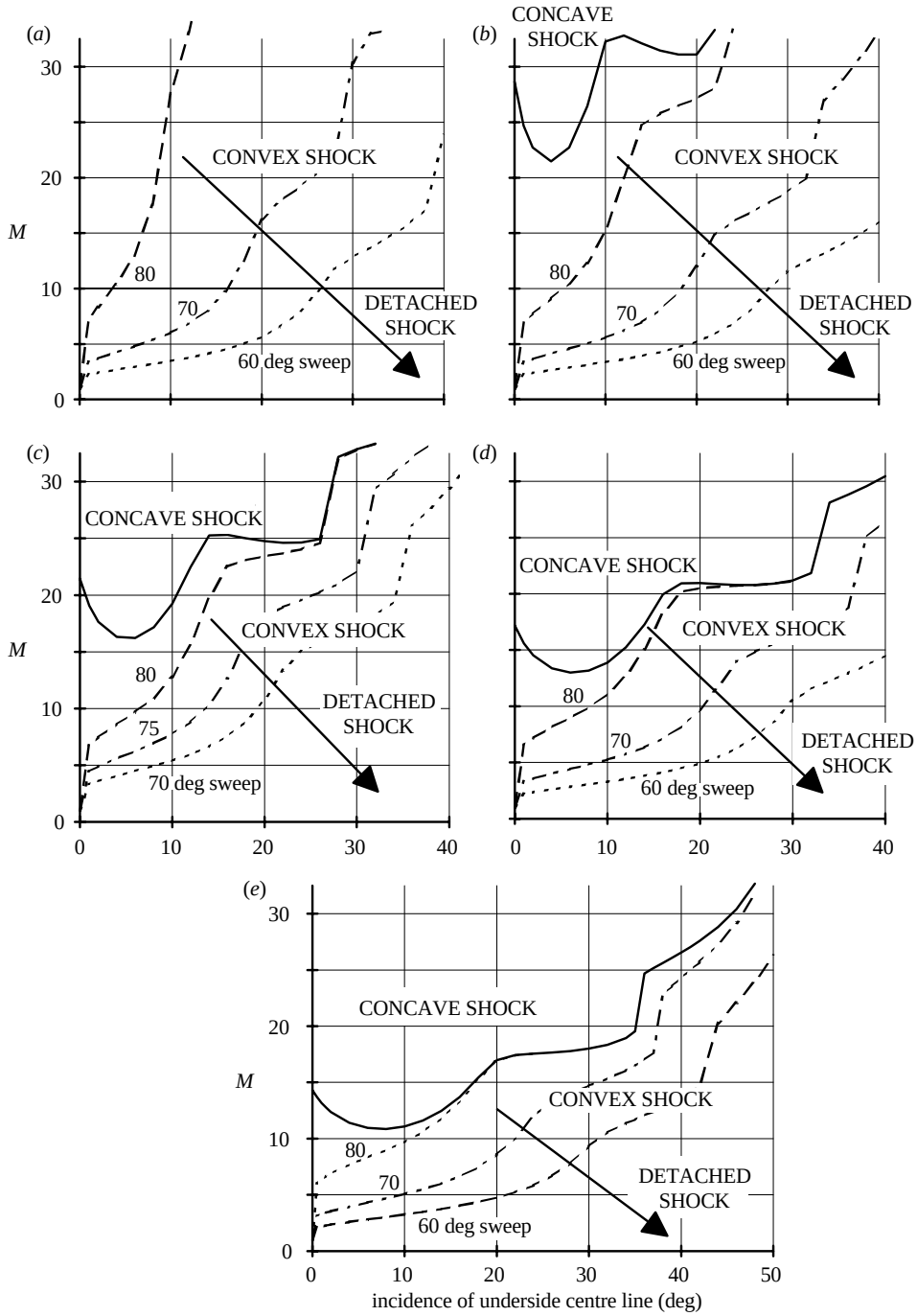

Figure 3. Effect of sweep and stand-off angle on the undersurface shock wave configuration of an inverted-V delta. Stand-off angles: (*a*) 0°; (*b*) 2°; (*c*) 2.67°; (*d*) 3.33°; (*e*) 4°. (The solid line denotes conditions for a plane undersurface shock. Dashed lines denote detachment of the shock from a leading edge of the designated sweepback.)

leading edges, and flow containment will be lost. This happens sooner for a highly swept delta than for one of lower sweep. Indeed, if the sweep is extremely high, an attached convex shock cannot exist.

The stand-off angle was originally selected as 2.67°, so that the aircraft could operate at the design condition from the start of the glide down to $M = 25$ when its design incidence is 17.4°. This incidence would be held constant as the Mach number decreases below 25, providing an attached convex shock right down to $M = 10$ for a 72° wing sweep. However, it was decided later that it was better instead to arrange the entire descent so that the incidence at any Mach number is just smaller than that which causes the (convex) shock to detach from the leading edge.

If one makes the choice of stand-off angle again with that knowledge, a higher value of more than $3\frac{1}{2}^\circ$ would seem preferable. This would allow the contained flow to be retained below $M = 10$, without any great difference in the incidence attainable at high M.

On the other hand, it could be contested that a flat-bottomed vehicle (that is, with zero stand-off angle) would be easier to construct. However, as will be seen from figure 3*a*, the lower surface flow is then contained by an attached shock only for $M > 16$, assuming an incidence of 17.4° (or more) and a wing sweep of 72°. It could be contained down to $M = 10$ by reducing the leading-edge angle (and so also the incidence) to *ca.* 13°, but this seems impractical. Alternatively, the same effect would be achieved if the sweep were decreased to 68°, though (with limited span) this inevitably reduces wing area and increases the wing loading. Moreover, any of these measures—increasing wing loading or reducing leading-edge angle, incidence, or sweepback—increase the leading-edge temperature. Clearly, therefore, the provision of a recessed underside serves a useful purpose, although this does need to be weighed against any disadvantage that it may cause.

The irregularity of the boundaries shown in figure 3 is due to the inclusion of real-gas effects, calculated on the assumption that the flight dynamic pressure q is 100 Pa. However, during the descent path ultimately preferred, q increases very markedly as M decreases (from *ca.* 200 Pa at $M = 28$ to *ca.* 3 kPa at $M = 10$). A revised representation takes this into account, but the general trends are not greatly altered.

4. Calculation of wing pressure distribution

During the chosen descent path, the incidence drops from *ca.* 35° at $M = 28$ to 17° at $M = 10$. It is necessary to compute the pressure distribution on the underside, ignoring that on the top surface, which is evidently in shadow.

If the wing is regarded as a delta with moderate inverted-V cross-section, it is possible, although not altogether easy, to compute the conical flow about the underside. However, as shown in figure 4*a*, there is a relatively small difference in pressure between the underside centre section and the wing leading edges. It was therefore felt adequate to compute the pressure along each ray through the wing apex by equating it with the pressure behind a shock wave that produces the undersurface deflection along that ray. This in turn always gave an average value close to the mean of the two pressures at the centre section and the tip, and finally that simple approximation was deemed acceptable, particularly bearing in mind that it needs to be applied to

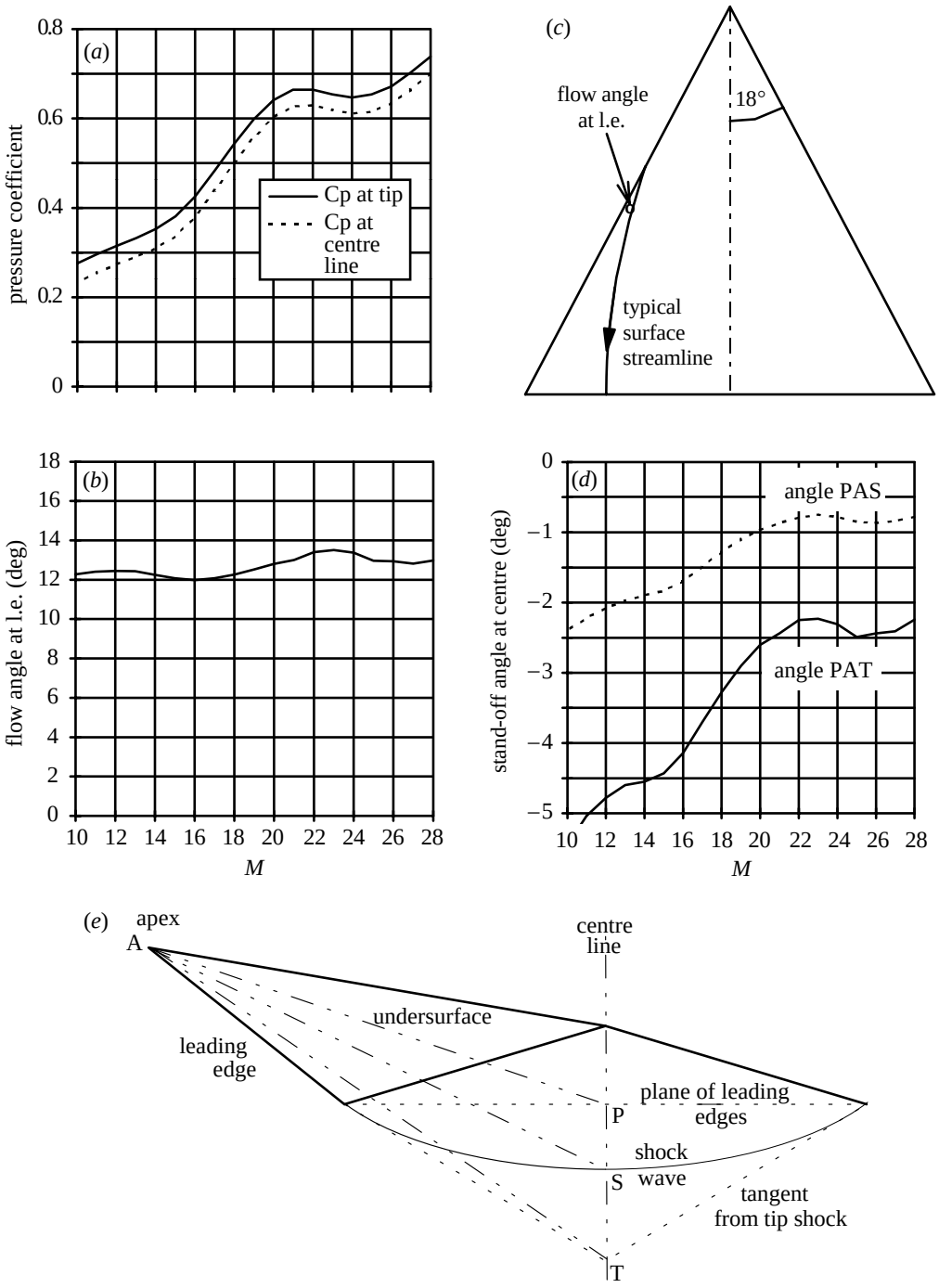

Figure 4. (*a*) Difference of pressure between leading edge and underside centre section. (*b*) Angle between surface flow and leading edge immediately downstream of leading-edge shock (see (*c*)). (*d*) Shape of convex shock (refer to diagram (*e*) for notation).

the *rounded* delta planform actually selected for SLEEC22 (figure 2), which does not have a conical flow field over its underside.

Figure 4*b* shows that the flow streamlines immediately downstream of the leading-edge shock are inclined at an angle of only 12° or so to the edge. This implies that they are initially deflected outwards, away from the underside centre section (which is inclined at the semi-apex angle of 18° to the leading edges), as shown in figure 4*c*. This surface outflow is due to the pressure gradient across the undersurface. It has the benefit of accentuating the thermal conduction of heat away from the leading edge. This is because the boundary-layer heat flux varies as $1/\sqrt{s}$, where s is measured along the surface streamline from the leading edge, and, consequently, the larger this outflow, the more rapidly it will decrease in the direction normal to the edge.

Finally, figure 4*d* provides an indication of the curvature of the shock wave over the undersurface. This will be seen to become more pronounced as the Mach number decreases.

5. Heat protection studies

(*a*) *Wing leading edges*

In the direction normal to its leading edge, the wing is wedge-shaped with an included angle of 42.1° (though only 17.4° is in the streamwise direction). Initial consideration of the heating levels led to the proposal that the first 2.5 cm (1 in) of this wedge normal to the leading edge should be solid niobium (i.e. columbium) backed by 11 cm (4.3 in) of solid graphite within a niobium skin. This was selected to provide the minimum possible leading-edge temperature. This minimum arises because adding more conducting material at the edge puts up its mass and the wing loading. This in turn increases the heat flux to the edge. The temperature becomes a minimum if this just offsets the benefit derived from the extra conducting material.

The mass of this maximal protection is 215 kg (475 lb) for the SLEEC of figure 2, and it was later considered to be too heavy. The reduced mass quoted in Appendix A, 91 kg (200 lb), assumes a 16 mm (0.64 in) wedge of niobium followed by 7 cm (2.8 in) of niobium-covered graphite. However, the larger mass of conducting material was assumed in computing the maximum leading-edge temperature T_{LE} quoted in figure 5*b* and the tabulations of the descent in table 1. A reduction of T_{LE} was also incorporated in these estimates to allow for the effect of leading-edge rounding. Existing studies suggest that an asymmetric nose shape with a maximum radius (in the lower quadrant) of *ca.* 5 mm may be optimal.

The distribution of conducting material also needs to be reconsidered to make best use of the reduced mass, with the material being tapered towards the back, rather than remaining solid. If this is done, it is believed that the maximum leading-edge temperatures may not be more than 50 °C or so above those quoted for the heavier mass.

Figure 5. Temperature distributions during the descent of SLEEC22. (*a*) Variation with time of the temperature of various parts of the wing beneath the cabin. (*b*) Variation with time of nose temperature (T_0), leading-edge temperature (T_{LE}) and reference temperature (T_1). (*c*) Ratio of temperature (T) to reference temperature (T_1) for various parts of the wing, as determined by their streamwise distance (x) from the wing's leading edge (except beneath the cabin, or where $T < 300$ K).

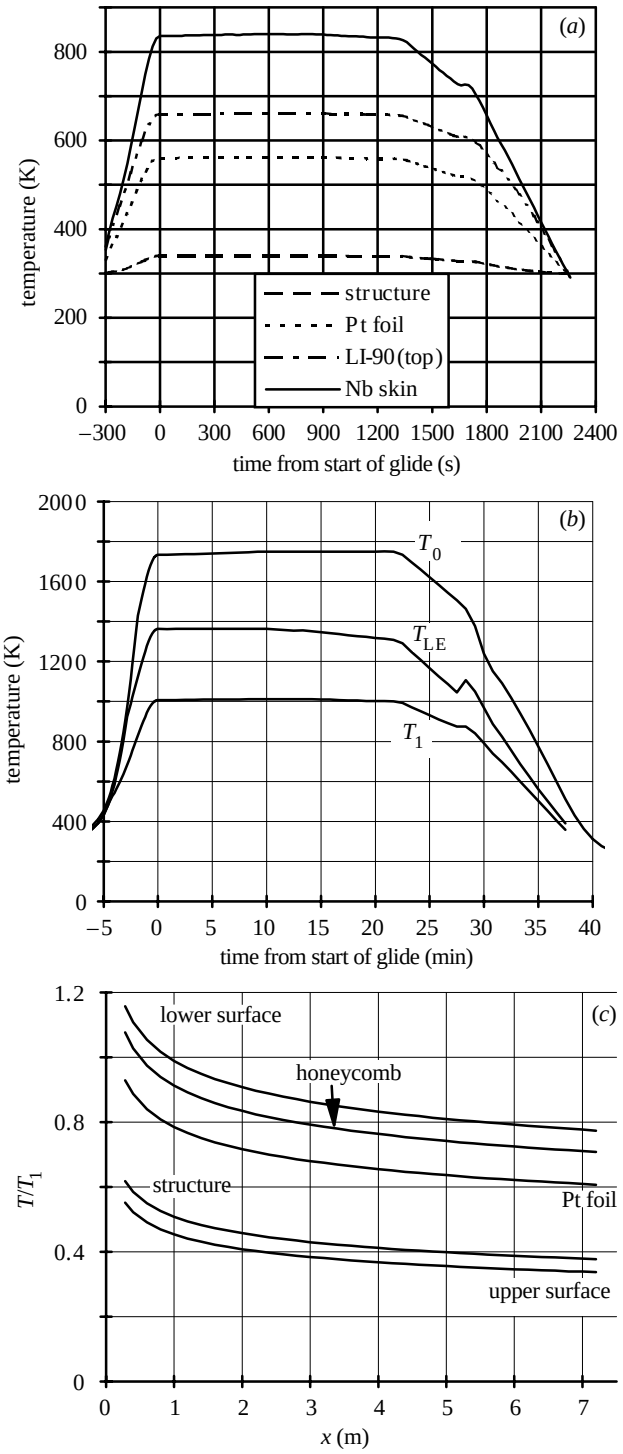

Figure 5. For description see opposite.

Table 1. *Detail of gliding descent of SLEEC22 (as at 21 May 1996)*
(Notation defined in Nomenclature section.)

t (s)	M	V (m s^{-1})	h (km)	$-\frac{\mathrm{d}h}{\mathrm{d}t}$ (m s^{-1})	X (km)	Y (km)	Φ (deg)	g	q (Pa)	C_{F} ($\times 10^3$)
0	28.00	7673	86.20	5.64	0	0	0.1	0.205	198	59.9
50	27.74	7608	85.89	6.73	377	2	0.6	0.211	205	58.3
100	27.45	7542	85.54	7.17	751	8	1.2	0.217	214	56.6
150	27.15	7474	85.17	7.55	1121	18	1.8	0.225	223	54.9
200	26.84	7403	84.79	7.69	1488	31	2.3	0.233	233	53.1
250	26.53	7331	84.40	7.98	1851	47	2.9	0.243	244	51.4
300	26.20	7256	83.98	8.68	2210	67	3.4	0.253	256	49.6
350	25.86	7179	83.53	9.22	2566	90	3.9	0.266	270	47.8
400	25.50	7097	83.06	9.66	2917	115	4.4	0.281	285	45.9
450	25.13	7010	82.55	10.79	3264	143	4.9	0.299	302	44.0
500	24.73	6919	81.98	11.85	3607	173	5.3	0.321	322	41.9
550	24.30	6819	81.37	12.72	3944	206	5.8	0.348	345	39.8
600	23.84	6712	80.71	13.60	4277	242	6.3	0.379	372	37.7
650	23.34	6594	80.01	14.73	4604	279	6.9	0.416	401	35.5
700	22.80	6465	79.22	16.68	4924	319	7.5	0.454	436	33.3
750	22.21	6326	78.34	18.51	5237	363	8.2	0.492	479	30.9
800	21.59	6177	77.37	20.50	5543	409	9.0	0.531	531	28.6
850	20.93	6021	76.30	22.04	5841	458	9.8	0.567	594	26.2
900	20.26	5860	75.15	23.60	6131	510	10.8	0.597	670	23.9
950	19.59	5698	73.97	24.02	6412	566	11.8	0.620	756	21.7
1000	18.94	5538	72.75	24.63	6684	625	12.8	0.639	857	19.7
1050	18.29	5381	71.49	26.96	6948	688	13.9	0.663	972	17.8
1100	17.60	5226	70.12	27.86	7204	753	15.1	0.696	1112	16.0
1150	16.92	5068	68.67	30.15	7451	823	16.6	0.740	1278	14.4
1200	16.23	4908	67.10	32.89	7688	897	18.4	0.795	1485	12.8
1250	15.52	4742	65.35	37.07	7916	977	20.8	0.864	1752	11.3
1300	14.79	4570	63.49	36.78	8132	1064	23.7	0.952	2076	9.92
1350	14.06	4386	61.74	20.65	8335	1159	27.3	1.046	2394	8.79
1400	13.38	4198	60.75	19.47	8524	1263	31.4	1.046	2485	8.19
1450	12.73	4015	59.77	19.84	8697	1375	35.7	1.046	2570	7.64
1500	12.09	3836	58.77	20.20	8855	1495	40.0	1.046	2654	7.14
1550	11.48	3662	57.75	20.51	8997	1619	44.4	1.046	2738	6.68
1600	10.88	3491	56.69	22.04	9123	1748	48.9	1.046	2830	6.24
1650	10.31	3326	55.55	23.52	9233	1879	53.4	1.046	2943	5.83
1700	9.76	3165	54.59	2.01	9329	2012	57.3	1.046	2988	5.99
1750	9.25	2987	55.40	−33.58	9412	2143	60.5	1.046	2418	6.51
1800	8.64	2751	58.00	−66.19	9484	2268	61.7	1.064	1500	7.70
1850	7.75	2483	56.87	69.46	9545	2384	65.3	1.028	1401	6.97
1900	6.83	2225	53.66	55.09	9597	2490	66.0	1.085	1646	5.66
1950	6.00	1980	50.90	52.20	9640	2587	69.1	1.077	1801	4.67
2000	5.31	1752	48.29	52.53	9673	2674	72.9	1.068	1951	3.83

PHILOSOPHICAL TRANSACTIONS OF THE ROYAL SOCIETY A MATHEMATICAL, PHYSICAL & ENGINEERING SCIENCES

Table 1. (*Cont.*)

t (s)	C_L	L/D	α (deg)	β (deg)	M_e	R_θ	R_c	T_0 (K)	T_{LE} (K)	T_1 (K)
0	0.545	1.21	34.8	74.6	8.26	128	4.38×10^4	1734	1363	1007
50	0.542	1.22	34.6	69.9	8.21	131	4.55×10^4	1734	1362	1007
100	0.540	1.23	34.4	64.5	8.15	134	4.73×10^4	1735	1363	1007
150	0.537	1.25	34.2	59.5	8.09	137	4.94×10^4	1737	1363	1008
200	0.535	1.26	34.0	54.4	8.03	140	5.17×10^4	1738	1363	1008
250	0.534	1.27	33.9	50.1	7.96	144	5.41×10^4	1739	1363	1009
300	0.533	1.28	33.8	45.9	7.90	147	5.67×10^4	1740	1363	1009
350	0.534	1.29	33.7	41.1	7.83	151	5.98×10^4	1742	1363	1010
400	0.535	1.30	33.7	38.0	7.75	156	6.31×10^4	1743	1363	1010
450	0.539	1.30	33.8	35.3	7.67	161	6.69×10^4	1744	1363	1010
500	0.543	1.31	33.9	32.5	7.59	166	7.16×10^4	1747	1363	1011
550	0.548	1.31	34.0	31.1	7.49	173	7.69×10^4	1749	1363	1012
600	0.555	1.31	34.3	30.3	7.39	179	8.29×10^4	1750	1363	1012
650	0.564	1.30	34.6	30.9	7.28	187	8.99×10^4	1750	1360	1012
700	0.567	1.31	34.7	31.1	7.16	196	9.82×10^4	1750	1357	1011
750	0.563	1.33	34.4	30.7	7.03	206	1.09×10^5	1750	1354	1011
800	0.552	1.36	33.9	30.9	6.89	218	1.22×10^5	1750	1356	1012
850	0.534	1.41	33.0	31.1	6.74	232	1.38×10^5	1750	1351	1011
900	0.507	1.49	31.7	29.6	6.58	248	1.59×10^5	1750	1347	1010
950	0.475	1.58	30.1	28.7	6.43	266	1.83×10^5	1750	1342	1009
1000	0.440	1.69	28.4	27.1	6.30	287	2.13×10^5	1750	1337	1007
1050	0.408	1.80	26.9	26.9	6.18	310	2.50×10^5	1750	1332	1006
1100	0.380	1.91	25.5	28.6	6.07	336	2.95×10^5	1750	1327	1005
1150	0.356	2.02	24.3	31.6	5.97	366	3.52×10^5	1750	1323	1003
1200	0.333	2.14	23.1	35.2	5.88	401	4.26×10^5	1750	1318	1002
1250	0.309	2.27	21.9	38.9	5.78	443	5.24×10^5	1751	1314	1002
1300	0.290	2.38	21.0	42.5	5.69	491	6.50×10^5	1749	1308	1000
1350	0.278	2.48	20.3	42.1	5.58	539	7.88×10^5	1734	1291	993
1400	0.269	2.55	19.8	44.1	5.47	564	8.64×10^5	1697	1249	972
1450	0.261	2.61	19.4	42.3	5.36	588	9.44×10^5	1660	1208	952
1500	0.253	2.69	18.9	40.5	5.24	614	1.03×10^6	1621	1167	931
1550	0.247	2.75	18.5	38.9	5.11	642	1.12×10^6	1583	1126	911
1600	0.239	2.84	18.0	37.4	4.97	671	1.22×10^6	1544	1086	892
1650	0.231	2.93	17.5	36.1	4.81	704	1.34×10^6	1506	1046	874
1700	0.228	2.27	22.4	22.9	4.06	721	1.32×10^6	1463	1107	874
1750	0.275	2.01	25.2	18.3	3.59	666	1.08×10^6	1378	1050	841
1800	0.415	1.47	33.4	5.0	2.59	522	6.00×10^5	1240	969	792
1850	0.426	1.46	33.7	5.0	2.44	536	6.32×10^5	1152	887	740
1900	0.391	1.61	31.1	5.0	2.55	632	9.07×10^5	1091	824	697
1950	0.362	1.78	28.7	5.1	2.60	716	1.19×10^6	1017	755	649
2000	0.336	1.96	26.4	14.6	2.61	804	1.53×10^6	940	688	600

PHILOSOPHICAL TRANSACTIONS OF THE ROYAL SOCIETY A MATHEMATICAL, PHYSICAL & ENGINEERING SCIENCES

Table 1. (*Cont.*)

t (s)	M	V (m s^{-1})	h (km)	$-\frac{dh}{dt}$ (m s^{-1})	X (km)	Y (km)	Φ (deg)	g	q (Pa)	C_F ($\times 10^3$)
2050	4.71	1540	45.76	49.08	9697	2753	76.3	1.063	2103	3.10
2100	4.16	1342	43.30	49.38	9713	2823	80.7	1.058	2247	2.49
2150	3.64	1158	40.81	50.17	9721	2885	85.6	1.054	2384	1.98
2200	3.14	987	38.27	51.46	9724	2938	88.4	1.051	2513	1.55
2250	2.68	829	35.66	53.21	9725	2983	89.6	1.049	2631	1.21
2300	2.25	685	32.95	54.93	9725	3020	89.9	1.048	2736	
2350	1.84	556	30.04	59.83	9725	3051	90.0	1.047	2829	
2400	1.49	446	27.01	61.31	9725	3076	90.0	1.047	2907	
2450	1.19	354	23.95	60.68	9725	3096	90.0	1.046	2972	
2500	0.95	282	20.98	57.62	9725	3112	90.0	1.046	3025	
2550	0.77	228	18.20	53.51	9725	3124	90.0	1.046	3070	
2600	0.64	188	15.66	48.01	9725	3135	90.0	1.046	3107	
2650	0.54	158	13.39	42.75	9725	3143	90.0	1.047	3137	
2700	0.46	137	11.36	38.61	9725	3151	90.0	1.052	3235	

(*b*) *Wing apex*

Even with an ample provision of material for conduction-assisted cooling, very high temperatures are reached if the port and starboard swept-wing edges are brought together at the sharp V-shaped apex of a delta wing. It is better to curve the edges gradually round to meet unswept in the central plane of symmetry (as shown in figure 2), even though this form of thermal protection becomes less effective as the edge sweepback is reduced. Extra conducting material then needs to be added to limit the apex temperature, and a modest nose radius incorporated into the design to limit the peak heat flux.

In the initial configuration discussed here, the nose radius at the planform apex was chosen as 5 cm (2 in), and the complete rounded nose was envisaged as solid graphite. As with the leading-edge design, this is capable of further improvement by (for instance) detailed shaping of the graphite filling, hollowing it out but extending it further downstream.

(*c*) *Internal structure and cabin*

The undersurface of SLEEC22 is supposed to be constructed of niobium sheeting, possibly in the form of separate rectangular plates. Its outer surface is 'blackened' to assist radiation cooling (its emissivity being taken as 0.85).

Its temperature could be reduced further by allowing radiation from its interior surface, so that the surface of the top skin, although in shadow and so not heated by the airflow, nonetheless also becomes a hot radiating surface. The internal wing structure would then necessarily become very hot (reaching temperatures of between, say, 650 and 900 K). However, for the time being at least, it is envisaged that a cooler structure would be preferred. This can be achieved by inhibiting the escape of radiation to the interior. The interior niobium surface would then need to be

Table 1. (*Cont.*)

t (s)	C_L	L/D	α (deg)	β (deg)	M_e	R_θ	R_c	T_0 (K)	T_{LE} (K)	T_1 (K)
2050	0.315	2.14	24.2	14.2	2.59	898	1.94×10^6	860	624	551
2100	0.296	2.28	21.8	13.6	2.53	995	2.40×10^6	775	562	502
2150	0.280	2.41	19.2	13.3	2.44	1091	2.90×10^6	688	502	453
2200	0.267	2.52	16.0	13.5	2.31	1183	3.40×10^6	599	445	405
2250	0.256	2.63	11.9	14.0	2.15	1270	3.90×10^6	511	391	358
2300	0.247	2.73	9.9	15.2		602		430		
2350	0.239	2.82	9.6	16.0		593		363		
2400	0.234	2.89	9.3	±16.3		587		313		
2450	0.229	2.95	9.1	±16.3		584		277		
2500	0.225	3.00	9.0	±16.4		583		253		
2550	0.222	3.04	8.8	±16.1		582		239		
2600	0.220	3.07	8.7	±16.2		581		232		
2650	0.218	3.09	8.6	±16.7		581		227		
2700	0.213	3.17	8.4	±18.3		580		224		

polished, and covered with a layer of highly polished (platinum) foil, from which it must be kept separated. The best way of maintaining this gap will need research. For the moment, the foil is regarded as supported on a honeycomb of wide pitch but shallow depth.

If a cool structure is preferred, the lower half of the pressurized shell forming the cabin (assumed to be maintained at 300 K) should be blackened, and a layer of insulation placed under the platinum foil in thermal contact with the underside niobium skin. About 3 cm (1.2 in) of LI-90 spread over 3.25 m^2 (35 ft^2) would limit the rise in cabin temperature during the whole descent to 2 K. The rate of heat input to the cabin is then *ca.* 440 W m^{-2} or 1.4 kW in total. The total heat input over the entire descent is *ca.* 0.77 kWh. It should be pointed out that these estimates omit the effect of thermal conduction from the structure supporting the cabin, and the heat transfer to or from its top surface, which, for much of the descent, may be losing heat by radiation.

Using the values determined from the descent detailed in table 1, the variation of the temperature under the cabin is shown in figure 5*a*, from which it is seen that the (average) structure temperature is only a few degrees above the cabin temperature.

Figure 5*b* shows the variation with time of the apex and leading-edge temperatures as calculated for the same descent, and the variation of a 'reference' temperature T_1, which scales the time variation of various parts of the structure as shown in figure 5*c*. As will be seen, T_1 is a little over 1000 K for most of the descent, and the average structure temperature (away from the cabin) is increased to between 400 and 600 K.

6. Boundary-layer calculations

With the surface pressure distribution known, and the form of internal construction affecting the skin temperature decided, it is possible to evaluate the boundary-layer characteristics of the flow beneath the underside. These computations were carried

out with the same model of real air as used for the shock-wave analysis, and assume the airflow to be in thermodynamic equilibrium. This latter assumption is quite inappropriate at the highest altitudes of the descent, particularly before the assumption of the steady glide, and, in that region, the results are simply rather rough overestimates of surface temperatures.

The other consideration that affects these boundary-layer calculations is the possibility of transition to turbulence. Bearing in mind the low pressure gradients existing over the lower surface, it was initially decided to treat values of $R_x > 2 \times 10^6$ or $R_\theta/M > 200$ as indicating the possibility of transition, where R_x is the local Reynolds number and R_θ is that based on momentum thickness. However, these inequalities are not triggered until $M < 5$, leading to the expectation that full-chord laminar flow should certainly be possible at all speeds for which the bottom surface flow is contained, and heating is important. Having stated that, it has to be admitted that the problem of forecasting transition is always contentious, and not least by Reynolds-number criteria like these. For instance, much will depend in practice on a reasonable surface condition being maintained.

In the study being reported, full-chord laminar flow is assumed, down to a Mach number of 10, where containment of the bottom surface flow is lost. These calculations lead to the assessment of a mean value of the skin friction coefficient (based on the values along the underside centre section) as well as to the surface temperatures, such as those shown in figure 5*b*. At lower Mach numbers, no attempt is made to calculate a pressure distribution, but a lift/drag polar is estimated to enable the description of the descent to be continued. In that context, the only temperature that can continue to be reliably estimated is that of the nose, T_0.

7. Choice of descent

A relation between incidence and Mach number is first chosen. Then, to achieve crossrange, the descent is regarded as a continuous turn, until the direction of motion has already been turned through a right-angle. The turn is restrained firstly by the imposed g limit on total acceleration, and, secondly, by the imposed limits on leading-edge temperature T_{LE} and nose temperature T_0, either of which can be reduced by easing off the sideways g (and climbing out of the turn). There is a certain amount of independence, within limits, between T_{LE} and T_0, because the former peaks at a higher Mach number than the latter.

In the initial part of the study it was envisaged that the incidence would be held at 17.4° down to $M = 10$, and this gave crossranges beyond 3000 km, but only at the expense of excessive values of T_{LE} and T_0. The altitude of the descent was, therefore, raised by selecting as high an incidence as is compatible with an attached shock. There might, of course, be no serious degradation of re-entry performance by going beyond that limit. It was imposed simply to allow reliable estimates of the aerodynamic and heat-transfer characteristics to be made, as we have already described. Figure 6 shows the variation of crossrange with the imposed temperature limits in this condition, subject also to an acceleration limit of $1.045g$ during the descent. Note that a range of 3000 km and more is still achievable, because the re-entry starts at a higher Mach number.

It also shows that the duration of the peak acceleration increases with T_0. This arises because the higher values of T_0 result from pulling higher g, and this causes the

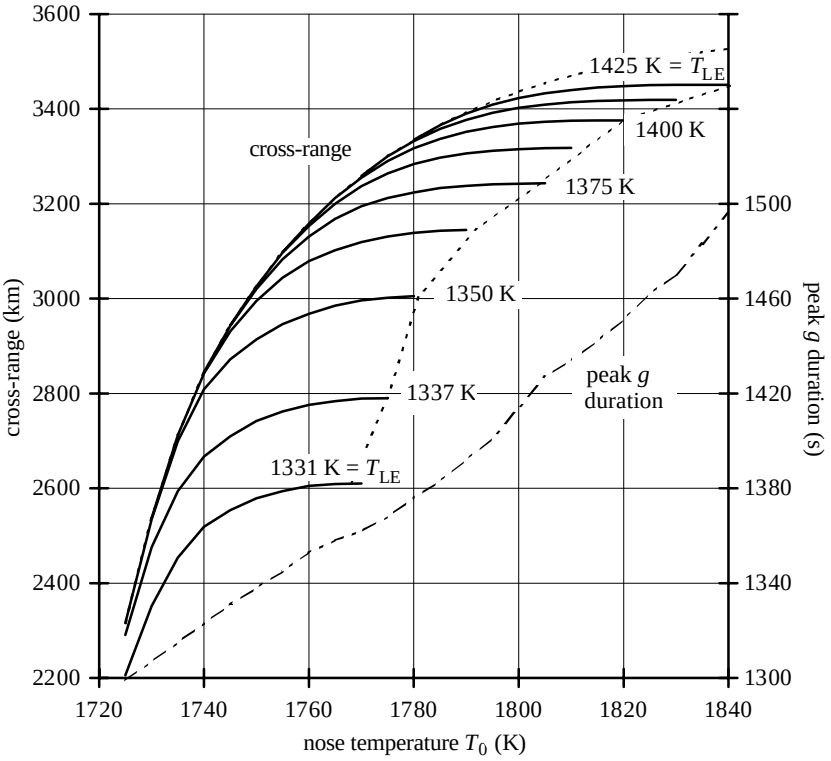

Figure 6. The effect of leading-edge temperature T_{LE} and nose temperature T_0 on crossrange and duration of peak deceleration (less than $1.045g$) on SLEEC22.

g limit to be imposed earlier on during the descent. A similar effect is not apparent with an increase of T_{LE} because its peak values occur much earlier in the descent, where the acceleration is nowhere near to becoming excessive.

8. Calculation of descent

The maximum temperatures to be imposed on the descent were chosen as $T_0 = 1750$ K and $T_{LE} = 1363$ K. The re-entering craft is supposed, initially, in a temporary parking orbit at a height of *ca.* 140 km. It is then retarded sufficiently so that it passes an altitude of 120 km at a rate of descent of 160 m s^{-1} (as does the Shuttle Orbiter), correctly aligned at an incidence of 34.5°. A thrust acceleration of $0.083g$, directed backwards and 10° downwards (to the underside centreline) is then supposed to be applied. As shown in table 2, this thrust, along with the developing lift on the vehicle, causes the rate of descent to slacken, and a pull-out acceleration to develop. This is redirected over the last 5 or 6 s, before the thrust is turned off, by rolling the craft over into a 76° bank. The reduced component of vertical lift is then adequate for the start of the glide.

It is quite possible to perform this manoeuvre without the use of thrust, but its provision was originally seen as a means of correcting any variation in the rate of descent at 120 m s^{-1}, or of dealing with the variability of air density at a height of 86 km, at which the glide starts. As used in the manoeuvre detailed in table 2, the

Table 2. *De-orbit and $M = 28$ pull-out of SLEEC22 (as at 3 October 1995)*
(Notation defined in Nomenclature section.)

t (s)	V (m s^{-1})	h (km)	$-\mathrm{d}h/\mathrm{d}t$ (m s^{-1})	X (km)	Y (km)	Φ (deg)	g
0.0	7551	141.37	0.00	0	0	0.00	0.000
30.0	7551	141.10	18.32	222	0	0.00	0.000
60.0	7552	140.27	36.62	443	0	0.00	0.000
90.0	7554	138.90	54.89	665	0	0.00	0.000
120.0	7556	136.98	73.10	887	0	0.00	0.000
150.0	7559	134.51	91.24	1109	0	0.00	0.000
180.0	7563	131.50	109.29	1331	0	0.00	0.000
210.0	7567	127.96	127.23	1553	0	0.00	0.000
240.0	7572	123.87	145.04	1776	0	0.00	0.001
265.4[a]	7576	120.00	160.00	1965	0	0.00	0.001 | 0.084
280.0	7588	117.66	160.15	2073	0	0.00	0.083
300.0	7603	114.46	159.76	2222	0	0.00	0.083
320.0	7619	111.27	158.66	2372	0	0.00	0.083
340.0	7634	108.12	156.77	2522	0	0.00	0.083
360.0	7648	105.01	153.99	2672	0	0.00	0.083
370.0	7655	103.48	152.19	2747	0	0.00	0.083
380.0	7662	101.97	150.06	2823	0	0.00	0.083
390.0	7669	100.48	147.57	2898	0	0.00	0.084
400.0	7675	99.02	144.63	2974	0	0.00	0.085
410.0	7681	97.59	141.16	3049	0	0.00	0.087
420.0	7686	96.20	137.05	3125	0	0.00	0.090
430.0	7691	94.85	132.19	3201	0	0.00	0.095
440.0	7695	93.56	126.44	3277	0	0.00	0.102
450.0	7698	92.32	119.64	3352	0	0.00	0.111
460.0	7700	91.17	111.64	3428	0	0.00	0.123
470.0	7701	90.10	102.30	3504	0	0.00	0.137
480.0	7701	89.13	91.51	3580	0	0.00	0.154
490.0	7699	88.27	79.20	3656	0	0.00	0.171
500.0	7696	87.55	65.41	3732	0	0.00	0.189
510.0	7692	86.97	50.28	3808	0	0.00	0.205
520.0	7687	86.54	34.06	3884	0	0.00	0.217
522.0	7685	86.48	30.72	3899	0	0.00	0.219
524.0	7684	86.42	27.36	3914	0	0.00	0.221
526.0	7683	86.37	23.98	3929	0	0.00	0.223
528.0	7682	86.33	20.57	3944	0	0.00	0.224
530.0	7680	86.29	17.16	3960	0	0.00	0.225
532.0	7679	86.26	13.73	3975	0	0.00	0.226
534.0	7678	86.23	10.30	3990	0	0.00	0.227
535.0	7677	86.22	8.59	3997	0	0.00	0.227
536.0	7676	86.22	7.20	4005	0	0.01	0.227
537.0	7675	86.21	6.47	4013	0	0.02	0.228
538.0	7675	86.20	6.05	4020	0	0.04	0.228
539.0	7674	86.20	5.76	4028	0	0.05	0.228
540.0	7673	86.19	5.56	4035	0	0.07	0.228
540.5[b]	7673	86.19	5.48	4043	0	0.08	0.228 | 0.205

[a]Thrust *on* (at $h = 120$ km).
[b]Thrust *off*; $\Delta V = 224$ m s^{-1}; t and X reset to zero for start of glide.

Table 2. (*Cont.*)

t (s)	q (Pa)	α (deg)	β (deg)	T_0 (K)	T_{LE} (K)	T_1 (K)
0.0	0.1	34.5	0.0	319	304	304
30.0	0.1	34.5	0.0	320	305	305
60.0	0.1	34.5	0.0	325	309	310
90.0	0.1	34.5	0.0	333	317	317
120.0	0.1	34.5	0.0	344	328	328
150.0	0.2	34.5	0.0	360	343	343
180.0	0.2	34.5	0.0	382	364	364
210.0	0.3	34.5	0.0	412	393	393
240.0	0.4	34.5	0.0	455	433	433
265.4[a]	0.6	34.6	0.0	507	482	483
280.0	0.9	34.6	0.0	547	521	512
300.0	1.4	34.6	0.0	614	585	543
320.0	2.3	34.7	0.0	696	663	578
340.0	3.9	34.7	0.0	792	754	616
360.0	6.7	34.8	0.0	906	863	660
370.0	8.8	34.8	0.0	970	924	683
380.0	11.5	34.8	0.0	1039	956	706
390.0	15.1	34.8	0.0	1111	989	730
400.0	19.7	34.9	0.0	1187	1022	755
410.0	25.6	34.9	0.0	1267	1056	780
420.0	33.1	34.9	0.0	1350	1090	805
430.0	42.3	34.9	0.0	1429	1124	830
440.0	53.5	34.9	0.0	1471	1157	855
450.0	66.8	34.9	0.0	1513	1189	879
460.0	82.2	34.9	0.0	1552	1220	902
470.0	99.6	34.9	0.0	1590	1250	923
480.0	118.4	34.9	0.0	1624	1277	944
490.0	137.8	34.9	0.0	1656	1302	962
500.0	156.6	34.9	0.0	1682	1323	977
510.0	173.4	34.9	0.0	1704	1340	990
520.0	186.6	34.9	0.0	1721	1353	999
522.0	188.7	34.9	0.0	1723	1355	1001
524.0	190.6	34.9	0.0	1725	1356	1002
526.0	192.3	34.9	0.0	1727	1358	1003
528.0	193.8	34.9	0.0	1729	1359	1004
530.0	195.0	34.9	0.0	1730	1360	1005
532.0	196.0	34.9	0.0	1731	1361	1006
534.0	196.8	34.9	0.0	1732	1362	1006
535.0	197.1	34.9	8.7	1733	1362	1007
536.0	197.3	34.9	48.9	1733	1362	1007
537.0	197.5	34.9	63.8	1733	1363	1007
538.0	197.7	34.9	69.4	1734	1363	1007
539.0	197.9	34.9	72.3	1734	1363	1007
540.0	198.0	34.9	74.1	1734	1363	1007
540.5[b]	198.1	34.9	74.7	1734	1363	1007

[a]Thrust *on* (at $h = 120$ km).
[b]Thrust *off*; $\Delta V = 224$ m s^{-1}; t and X reset to zero for start of glide.

equivalent velocity increment due to the rocket thrust is 224 m s^{-1}. Accordingly, the amount of propellant required would be *ca.* 10% of the mass. This is comparable with the rocket impulse likely to be required in de-orbiting. Whether such a provision is really essential, and how much propellant might *in extremis* be required, needs further consideration, but our current opinion is that it is *not* needed. However, a study does need to be made of the influence of this entire de-orbiting manoeuvre on the attainable touchdown accuracy.

Finally, in table 1, we provide full detail of the gliding descent of SLEEC22, and the Nomenclature section opposite defines the notation used in both the tables. The calculation incorporates a simulated control system whereby the craft is made to conform both with a prescribed descent path and the required variation of incidence with Mach number. To simplify this system (at least for the purpose of calculation) any spatial errors detected in the descent path are corrected by variation of the angle of bank, independently of the continuing change in the longitudinal trim.

When flow containment is lost, at an incidence of *ca.* 17° at $M = 10$, the aircraft is put into a short climb. This increases the incidence and reduces the aerodynamic heating to the upper surface that then threatens to become significant, because of the spill of air round the leading edge. In order not to exceed the acceleration limit (because of the higher drag), the incidence has subsequently to be reduced and reaches 17° again at *ca.* $M = 3$, when, however, the problems of heating are virtually all over.

The ground track is turned through 90° by the time the speed has dropped to $M = 2$. The angle of bank after that time is assumed to change periodically in sign so that the crossrange is further increased. It will be realized that if the maximum crossrange is not required, then a similar descent path could, nonetheless, still be followed like that described here, but with frequent roll reversals, to keep the craft weaving about the desired ground track.

The detail of the descent is not carried below $M = 0.5$. Assuming a $C_{L_{max}}$ of (say) 1.2, the landing speed is 31 m s^{-1} (100 ft s^{-1}), and the maximum crossrange would be close to 3200 km. However, it would never be practical to use this full range, and the development of SLEEC22 to provide a high L/D at low speeds would be of much more value in improving its airfield approach characteristics than in increasing its range.

By way of conclusion, it can be observed that SLEEC22 provides a completely novel approach to the problem of re-entry. It has some very attractive features, although some are yet unproven, that are mostly derived from its low wing loading. There appears to be a strong case for continuing the current project study.

Appendix A. Dimensions and masses of SLEEC22

(*a*) *Dimensions (with underside centreline as datum)*

Overall length	8.79 m (28.8 ft)	Overall height	1.49 m (4.88 ft)
Wing root chord	7.32 m (24 ft)	Wing span	4.42 m (14.5 ft)
Tip chord	0.99 m (3.25 ft)	Wing area	20.2 m^2 (217.6 ft^2)
Leading-edge sweep	72°	Trailing-edge sweep	14°
Leading-edge angle	17.4°	Wing aspect ratio	0.966

Inclination of datum line to plane of leading edges	2.67°	Fin sweepback	72.6°
Fin mean chord	1.82 m (5.96 ft)	Total fin area	5.04 m^2 (54.3 ft^2)

(*b*) *Mass distribution in glide (estimate as at 4 June 1996)*

Thermal protection system (TPS):			
Apex	50 kg (110 lb)		
Wing leading edges	91 kg (200 lb)		
Beneath cabin	14 kg (30 lb)		
Tail fins	27 kg (60 lb)		
Total TPS mass		182 kg (400 lb)	(13%)
Structure:			
Wing	494 kg (1090 lb)		
Tail fins	50 kg (110 lb)		
Landing skids	45 kg (100 lb)		
Total structure mass		589 kg (1300 lb)	(42%)
Systems:			
Propulsion (RCS and propellant)	55 kg (120 lb)		
Primary power	62 kg (137 lb)		
Electrical conversion and distribution	31 kg (69 lb)		
Actuators	15 kg (34 lb)		
Avionics	122 kg (268 lb)		
ECLS	78 kg (172 lb)		
Recovery and flotation	45 kg (100 lb)		
Total controls and systems		408 kg (900 lb)	(29%)
Cabin:			
Pressurized shell (7.33 m^2 (79 ft^2) surface area)	23 kg (50 lb)		
Interior fittings	23 kg (50 lb)		
Occupants (2)	181 kg (400 lb)		
Total cabin and occupants		227 kg (500 lb)	(16%)
Total mass		1406 kg (3100 lb)	(100%)

Nomenclature

List of notation used in tables 1 and 2.

M	free-stream Mach number
t	time from start of de-orbit or glide (s)
V	aircraft speed (km h^{-1}) (1 km h^{-1} = 0.54 knots)
X, Y	distance travelled along, and at right-angles to, initial great-circle ground track projected onto the Earth's surface (km) (1 km = 0.54 nautical miles)

Φ	change of azimuth of ground track direction relative to initial direction (deg)
g	g loading of vehicle (aerodynamic force/aircraft mass) relative to standard sea-level free fall g ($9.806\,65\ \mathrm{m\,s^{-2}}$)
q	free-stream dynamic pressure (kPa) ($1\ \mathrm{kPa} = 20.9\ \mathrm{lbf\,ft^{-2}}$)
C_F	total skin friction coefficient for laminar flow, based on wing area
C_L	lift coefficient
L/D	lift-to-drag ratio
α	incidence of underside ridge line (deg)
β	angle of bank (deg)
M_e	local Mach number downstream of apex
R_θ, R_c	local Reynolds numbers at trailing edge of underside ridge line, based, respectively, on local momentum thickness θ, and root chord c
T_0	temperature at (unswept, sharp-edged) apex (K)
T_LE	temperature at (swept, sharp-edged) outboard leading edges (K)
T_1	'scale' temperature: i.e. the radiation equilibrium temperature (assuming emissivity = 0.85) on underside ridge line at 1 m from apex (K)

References

Nonweiler, T. R. F. 1959 Aerodynamic problems of manned space vehicles. *J. R. Aero. Soc.* **63**, 521.

Nonweiler, T. R. F. 1990 The waverider wing in retrospect and prospect—a personalised view. In *First Int. Hypersonic Waverider Symp., University of Maryland, MD, USA*.

Nonweiler, T. R. F., Wong, H. Y. & Aggarwal, S. R. 1971 The role of heat conduction in leading edge heating. *Ing. Arch.* **40**, 107.

Smith, B. 1999 X-38 test combines two flight modes. *Av. Wk. Sp. Tech.* **150**, 32–34.

Stone, H. W. & Piland, W. M. 1993 21st century space transportation system design approach: HL-20 personnel launch system. *J. S. R.* **30**, 521–528.

Walberg, G. D. 1991 Hypersonic flight experience. *Phil. Trans. R. Soc. Lond.* A **335**, 87–224.

Yoler, Y. A. 1961 Dynasoar—a review of the technology. *Aero. Engng* **20**, 8–67.